LAWRENCE
LIVERMORE
NATIONAL
LABORATORY

LLNL-JRNL-831119

Assessing the Effectiveness of Generalized Likelihood Ratio Test Detector Schemes in Seismic Event Detection and the Avoidance of Non-Target Signals

R. E. Vieceli, D. A. Dodge

January 25, 2022

Bulletin of the Seismological Society of America

Disclaimer

This document was prepared as an account of work sponsored by an agency of the United States government. Neither the United States government nor Lawrence Livermore National Security, LLC, nor any of their employees makes any warranty, expressed or implied, or assumes any legal liability or responsibility for the accuracy, completeness, or usefulness of any information, apparatus, product, or process disclosed, or represents that its use would not infringe privately owned rights. Reference herein to any specific commercial product, process, or service by trade name, trademark, manufacturer, or otherwise does not necessarily constitute or imply its endorsement, recommendation, or favoring by the United States government or Lawrence Livermore National Security, LLC. The views and opinions of authors expressed herein do not necessarily state or reflect those of the United States government or Lawrence Livermore National Security, LLC, and shall not be used for advertising or product endorsement purposes.

Assessing the Effectiveness of Generalized Likelihood Ratio Test Detector Schemes in Seismic Event Detection and the Avoidance of Non-Target Signals

Rhiannon E. Vieceli[1,2] and Douglas A. Dodge[2]

1 New Mexico Institute of Mining and Technology

2 Lawrence Livermore National Laboratory

Rhiannon E. Vieceli

Earth and Environmental Science Department

New Mexico Institute of Mining and Technology

801 Leroy Place

Socorro, New Mexico 87801

rhiannon.vieceli@student.nmt.edu

(R.E.V.)

Declaration of Competing Interests

The authors acknowledge there are no conflicts of interest recorded.

Rhiannon E. Vieceli is the corresponding author.

Abstract

Cross-correlation techniques have played a longstanding and pivotal role in seismic event monitoring. However, the performance of correlation-based detectors is challenged by nuisance seismicity, or non-target signals. Such detections are a problem when the mission is to automatically map events to the correct source region. Using aftershocks of the 2014 M_w 6.0 South Napa, California earthquake, we demonstrate the effectiveness of utilizing a dynamic correlation processor (DCP) framework in a Generalized Likelihood Ratio Test (GLRT) detector configuration to minimize non-target detections. A GLRT maximizes a detection statistic with respect to one or more unknown parameters. In this case, the detection statistic is a template signal match against the waveform in a window sliding over a data stream and the unknown parameter is an index variable indicating group membership of the template event or events. Detected events are assigned to the event group that yields the largest detection statistic. Our results show that a GLRT detector will outperform a suite of independently operating correlation and subspace detectors in terms of having a lower non-target detection rate at a given missed detection rate. We also show that a GLRT detector composed of a few high-rank subspace detectors has a slightly higher non-target detection rate, but a significantly lower missed detection rate than a GLRT detector composed of many low-rank subspace detectors. The high-rank GLRT configuration produced impressive results even with marginal data (single channel, single station, and very low time bandwidth product) which bodes well for the utility of building efficient aftershock classification systems and global monitoring systems at larger scales. However, future work is required to assess performance at regional scale and to assess the performance of the system at detecting target events not used in detector template creation.

Introduction

It has been a long-standing observation that seismic events occurring in close spatial proximity can produce very similar seismograms at nearby recording stations (e.g., Geller and Mueller, 1980; Schaff and Richards, 2004; Dodge and Walter, 2015). This waveform similarity can be exploited to detect and characterize additional seismicity. For example, the measurement of waveform similarity (correlation) between known events (template events) and an incoming waveform data stream can be used to find previously uncatalogued events, usually with better results in terms of greater numbers and more precise locations than more traditional techniques such as power detectors (e.g. Fremont and Malone, 1987; Harris, 1991; Hauksson and Shearer, 2005; Schaff, 2009; Cleveland and Ammon, 2013; Slinkard et al., 2014; Dodge and Harris, 2016, Harris and Dodge, 2021). However, not all closely located events will produce seismograms that correlate above a detection threshold, and it is also possible that noise and more distant seismic events will correlate with template events, complicating the use of correlation as an event detection and characterization tool.

Correlation-based seismic detectors implement a binary hypothesis test where observed data are assumed to be either entirely noise (null hypothesis) or else target signal plus superimposed noise. In the context of this binary hypothesis, a false alarm is the identification of noise as the target signal. In addition to false alarms, under certain scenarios, correlation detectors are subject to an additional problem; the detection of non-target (nuisance) signals.

Non-target signals may be artifacts (e.g., data spikes), but are also often generated by real seismic sources having seismograms near the target in signal space. What constitutes a non-target signal is dependent on the goal of running the detector algorithm. For example, a

correlation detector intended to monitor events from a specific mine might trigger on signals produced by explosions at nearby mines or signals from local earthquakes. These would be non-target detections. In contrast, if the goal were to detect explosion or earthquake signals from the entire mining region, then such detections would be correct.

Non-target signals can challenge the performance of correlation detectors, especially when the target events are small (magnitude < 2) (Carmichael, 2016; Carmichael and Hartse, 2016). Carmichael and Hartse (2016) addressed the problem of nuisance signals by incorporating non-target signals into the null hypothesis. However, their method required inflated thresholds to maintain desired false alarm rates. While higher thresholds achieve acceptable false alarm rates, they also lower detection rates. Nevertheless, theirs may be the best approach when operating a single correlation detector in an environment with significant nuisance seismicity.

An alternative approach to this problem was introduced by Harris and Dodge (2011). They implemented a system, later described as a dynamic correlation processor (DCP), that could build correlation detectors automatically from detections produced by one or more power detectors. In their system detectors compete with one another such that detected signals are assigned to the detector whose template best matches the signal.

The goal of Harris and Dodge (2011) was to demonstrate the potential for automatically categorizing aftershocks during an ongoing sequence. Kvaerna et al. (2014) investigated this concept further using a DCP to process aftershocks from the 2005 Kashmir and the 2012 Sumatra sequences. They found that correlation detectors were relatively ineffective at organizing the aftershock waveforms in a manner that could aid automatic processing. However, they noted that expansions of correlation detectors, known as subspace detectors (Harris, 2006),

that were built using many template events from diverse subsets of the aftershocks were effective in detecting many aftershocks not included in detector creation and that these detectors were also unlikely to detect events outside the geographic region of their particular subset. The Kvaerna et al. (2014) results suggest that if the target region used to create a subspace detector is large enough (tens to 100s of km) and if the events in that region provide a sufficient sampling in position and mechanism, then a highly sensitive subspace detector can be built that could potentially serve as a primary detector in a global monitoring system.

Standard practice in global monitoring pipelines is to use power detectors to produce detections (phase label, time, amplitude, etc.) for individual data streams. These detections are passed to a global associator that organizes them into common sources (events). The results of the automatic system are reviewed by human analysts, and after review, a significant fraction of automatically built events are often found to be improperly built. Deconstructing these false events and building events that were missed by the automatic system is time consuming and resource intensive.

If instead detections could be reliably mapped to geographic regions, then the association process could be made more robust. Hypotheses might be limited to just the associated regions or else might be weighted to favor the associated regions. This could be accomplished with a system in which the primary detector at each station is composed of multiple highly flexible subspace detectors, each built using events from a specific geographic region. The set of regions for which constituent detectors have been built would constitute the domain of the detector.

When events occur within the domain, one or more of the component subspace detectors would trigger, and the trigger having the highest detection statistic would be declared as the system detection. A system like this might be referred to as a “matched region detector” and its detection

strategy of composite hypothesis testing is known as a Generalized Likelihood Ratio Test (GLRT). The matched region detector, shown schematically in Figure 1, would be in many ways analogous to a correlation detector in that it identifies both the presence and the identity of a signal of interest. The difference would be in the size of the detector "footprint." Single channel correlation detectors have footprints less than a few hundred meters and even large multi-channel detectors have footprints less than a few kilometers (Ringdal et al., 2008). By contrast, a matched region detector could have a footprint of many tens of kilometers.

Many technical challenges would have to be met in creating a matched region detector, but a foundational problem is ensuring that the mapping of detections to source regions is robust. As with a correlation detector, it is important to characterize:

1. False Alarm rate (detections where only noise is present)
2. Missed Detection rate (target signal was present but no detection was declared)
3. Non-target detection rate (detection declared for signal originating in a non-target region)

Additionally, the component subspace detectors must be capable of detecting a large fraction of the events within their target region that were not used in detector creation.

In this work, we create a miniature matched region detector using data from the 2014 Napa aftershock sequence as a proxy for the larger-scale regional detector just described. We use this model to investigate the non-target detection rate.

We use the double-difference earthquake catalog of Hardebeck and Shelly (2016) as ground truth (GT) and study the behavior of four different detector configurations. The precise double-difference locations provide quasi ground truth, and because the clusters have inter-cluster

spacing on the order of their diameters, the scenario provides a good test of the robustness of the GLRT approach (at least at the scale of this problem).

Methods

Experimental Design

Our goal is to maximize the probability of detection within the target region while simultaneously minimizing the probability of misclassification. To this aim, using the Hardebeck and Shelly (2016) events grouped into 12 subregions, we tested four matched region detector configurations: 1) 12 high-rank subspace detectors operated independently, 2) the same 12 high-rank subspace detectors operated as a GLRT, 3) 664 low-rank subspace detectors operated independently, and 4) the same 664 low-rank subspace detectors operated as a GLRT. The high-rank and low-rank detectors were created from essentially the same event populations, but grouped differently. We divide these configurations into two experiments; Configurations 1 and 2 comprise the first, and Configurations 3 and 4 comprise the second. “Rank” is defined in the following discussion on subspace detectors. In the GLRT scenario, the goal is to ensure that the collection of correlation/subspace detectors pass a single detection per event on to the associator. In the competing scenario, those same detectors operate independently and pass their separate lists of detections on to the associator. Assessment and comparison of these four configurations addresses two distinct issues: the detection results 1) of GLRT vs. non-GLRT operation, and 2) performance when subregions are characterized by single high-rank detectors vs. many low-rank detectors.

Correlation and Subspace Detectors

Correlation-based seismic detectors operate on the foundation of a binary hypothesis test where discrete-time data in question **x** are determined to be either entirely noise (null hypothesis H_0) or a combination of noise **η** and signal of interest **s** (alternative hypothesis H_1)

$$\boldsymbol{x} = \boldsymbol{\eta} \quad \text{under null hypothesis } H_0,$$

$$\boldsymbol{x} = \boldsymbol{s} + \boldsymbol{\eta} \quad \text{under alternative hypothesis } H_1.$$

The noise is assumed to be zero-mean, white, and normally distributed with unknown variance σ^2 (power; σ is the standard deviation). Signals of interest are assumed to be deterministic, but scaled by an unknown amount A relative to a known template signal **u**

$$\boldsymbol{s} = A\boldsymbol{u} .$$

Correlation detectors require prior knowledge of the target, or template, signal and can only detect signals from within a limited footprint.

Like correlation detectors, subspace detectors can be used to scan a continuous data stream looking for matches to previously recorded signals. However, subspace detectors perform the matching operation by comparing the stream to a linear combination of basis vectors. The basis is created by choosing a set of template waveforms that sample an extended source region, performing a singular value decomposition (SVD) on the aligned signals, and retaining the first N left-singular vectors corresponding to the N largest singular values. The size of the basis is called the rank of the detector. A rank one subspace detector is simply a correlation detector: higher ranks indicate the use of multiple templates. The higher the rank the more flexible the detector is in detecting signals not part of the target set used in its creation (i.e., high-rank

subspace detectors are more sensitive to signals in the source region that have not been previously identified). The ability to match new signals using linear combinations of the basis vectors allows subspace detectors to detect some events that would be missed by correlation detectors built from the same events. However, the increased flexibility results in a higher false alarm rate at a given threshold.

Generalized Likelihood Ratio Test

The Generalized Likelihood Ratio Test (GLRT; Neyman and Pearson, 1928) has been widely implemented in the fields of electrical engineering and signal processing, particularly for applications regarding remote sensing (e.g. Wang, 2020; Wang and Li, 2020; Kim et al., 2019), and biotechnology (e.g. Kim et al., 2017) and medical-related (e.g. Chen et al., 2020; Nan and Nowak, 1999) applications. However, this statistical approach to data analysis has not yet been widely applied to seismic event detection. The GLRT operation is computationally expensive and the necessary compute infrastructure to support large-scale implementation is only becoming available with the advent of big-data computing. Previous seismic studies implementing the GLRT relied heavily on simulations and/or very small datasets (e.g. Fisk et al., 1993; Gray et al., 1996; Taylor and Hartse, 1997).

Recall that correlation-based seismic detectors implement a binary hypothesis test. Since signal models under the null hypothesis are special cases of those under the alternative hypothesis (i.e., the two models are nested), the detection rule is a likelihood ratio test.

Likelihood ratio tests (LRTs) compare the probability that the observed data are fit better by the more complex model (alternate hypothesis H_1) to the probability that the observed data are better explained by the simpler model (null hypothesis H_0)

$$\Lambda(\boldsymbol{x}) = \frac{p(\boldsymbol{x}|\mathrm{H}_1)}{p(\boldsymbol{x}|\mathrm{H}_0)}\,.$$

A threshold γ is chosen and the likelihood ratio is compared to it:

$$\Lambda(\boldsymbol{x}) > \gamma \quad \text{declare } \mathrm{H}_1,$$

$$\Lambda(\boldsymbol{x}) < \gamma \quad \text{declare } \mathrm{H}_0.$$

However, all parameters must be defined. When the problem involves unknown parameters (e.g., noise variance σ^2 and scale factor A), their values in the probability density functions for each hypothesis in the LRT can be replaced by their maximum likelihood estimates (MLEs), giving the Generalized Likelihood Ratio Test (Neyman and Pearson, 1928):

$$\widehat{\Lambda}(\boldsymbol{x}) = \frac{\max\limits_{\mathrm{A},\sigma} p(\boldsymbol{x}|H_1)}{\max\limits_{\sigma} p(\boldsymbol{x}|H_0)}\,.$$

$$\widehat{\Lambda}(\boldsymbol{x}) > \gamma \quad \text{declare } \mathrm{H}_1,$$

$$\widehat{\Lambda}(\boldsymbol{x}) < \gamma \quad \text{declare } \mathrm{H}_0.$$

Without the need to define all parameters a priori, the GLRT is an enhancement of the LRT.

Note that the above statistical approaches have been explained in the context of a basic correlation detector where there is a single template waveform and single target signal being searched for. This method has been expanded for use with subspace detectors and the case where there are multiple target signals (Harris and Paik, 2006; Harris, 2019).

Dynamic Correlation Processor

The dynamic correlation processor (DCP) was introduced by Harris and Dodge (2011) (see also Dodge and Harris, 2016) to autonomously create correlation and subspace detectors from a waveform data stream, and thenceforth apply those detectors to the data stream to detect similar signals. The software has been released as open source under the name Detection Framework Testbed and Toolkit (DFTT). In addition to operating as a dynamic correlation processor, DFTT can be operated as a conventional (static) correlation processor and can also be used to build and operate detectors based on bulletins of events (see Data and Detector Construction sections).

Data

Our experimental matched region detector is built using data from the aftershock sequence of the 2014 M_w 6.0 South Napa, California earthquake. We use as epicenter ground truth the double-difference earthquake catalog of Hardebeck and Shelly, 2016 (hereinafter referred to as H&S). Their catalog includes 1258 events comprised of 344 relocated Northern California Seismic Network (NCSN) catalog events, 913 of their additionally detected events, and the mainshock. Hardebeck and Shelly (2016) noted that the epicenters of the sequence visually form 12 distinct clusters distributed along the length of the fault zone. We omit the mainshock and note that there are outlier events that are not included in the H&S clusters. Based on these observations we applied K-means clustering to 1194 H&S epicenters to similarly produce 12 clusters; see Figure 2. These clusters serve as the target geographic regions of our experimental matched region detector. Table S1 in the Electronic Supplement lists the clusters and the number of events for each cluster.

We note that cluster definition depends on the goal of the work. Here, we aim to assess the performance of GLRT detectors compared to independently operating subspace and correlation detectors with less emphasis on geologic implications. Thus, our defined clusters are somewhat arbitrary. As our results show, the overlap of some clusters (e.g., clusters 5-9) does not seem to greatly impact the results between clusters in terms of non-target and missed detection rates. Clusters could be more systematically defined based on a correlation threshold or specific geologic regions. The key point for cluster creation is to ensure the subspace detector bases are representative of the target signals.

We used continuous waveform data from station NHC of the Northern California (NC) network. As shown in Figure 2, this station is located just off the West Napa fault zone approximately 4 km northwest of the main shock epicenter. NHC is close enough to the main body of aftershocks so that most seismograms have high signal-to-noise ratio (SNR). Because NHC is close to the fault zone there are significant variations in signal complexity and duration which map into significant variations in the correlation statistic behavior from cluster to cluster. The waveform data extend from 24 August 2014 to 30 November 2014 and are filtered 2 – 30Hz.

Detector Construction

By limiting the signal space from which detectors are built to bulletin events instead of allowing the framework to dynamically create correlation and subspace detectors, we ensure that the detector is matched to our test region and does not contain signals from other sources. (This is true to the extent that the curated bulletin-derived signal windows contain only target signals.)

For each cluster, we used DFTT to create a subset of extracted templates corresponding to the cataloged cluster events. For each catalog event with sufficient SNR, the software saved pointers

to a waveform segment extending from the P-arrival to the end of the coda (usually about 3 - 5 seconds). After all clusters were processed, we used the editing capability built into DFTT to create from the saved detections, correlation and/or subspace detectors for each cluster using only signals with clear signal onsets and no evidence of multiple arrivals. The subspace detector dimensions were set automatically by DFTT using a 90% energy capture threshold, meaning that 90% of the energy in all the input signals was reproduced in the detector basis signals. For Configurations 1 and 2, one subspace detector was created per cluster, resulting in 12 high-rank subspace detectors (independently operating for Configuration 1, and used together as a GLRT detector for Configuration 2). For Configurations 3 and 4, DFTT was allowed to create subspace and correlation detectors based on the catalog event times of each cluster, resulting in 664 low-rank detectors across all 12 clusters. The GLRT detector creation process is illustrated schematically in Figure 3.

The results of detector production for Configurations 1 and 2 are shown in Table1 and the results of detector production for Configurations 3 and 4 are shown in Table 2. There were 9 bulletin events that occurred during NHC data gaps for clusters 1,2,6,9,10. The cluster event count values in these tables have been adjusted to account for these missing data. For Configurations 1 and 2, only about 74% of the signals predicted by the H&S catalog were retained for detector creation and the rank of the detectors created from that set ranged from 15 to 61. The distance from NHC to the 12 cluster centroids ranged from under 2 km to nearly 16 km. The resulting variation in signal duration and complexity is reflected in the template time bandwidth product (TBP) which ranged from 0.68 to 19.81. As an example, Figure 4 shows the basis vectors for the cluster 6 subspace detector used in Configurations 1 and 2. The TBP can be thought of as the product of the “spread” of the signal vectors in the time and frequency domains, and for a given TBP the

number of distinct signals that can be resolved is at most a constant times the TBP. Thus, detectors with low TBP bases are more likely to detect non-target signals at a given threshold. At the short distances used in this experiment, the signal complexity (and hence TBP) increases with distance because the amount of scattered energy (coda) increases with distance.

After creation of each of the four configurations the suite of detectors was run over the data stream (24 Aug – 30 Nov) to produce the detections discussed in the next section.

Processing Results

We note that the DFTT software naturally operates as a GLRT detection system when more than a single detector is in place. However, DFTT saves all output from individual detectors in addition to the final detections. Individual detections are stored as "triggers" in DFTT parlance. This allows comparison of subspace detector performance (triggers) when operated individually to performance when operated as a component part of a GLRT detector (detections).

For each detector we would like to calculate the missed detection rate β (target signal present but no detection declared)

$$\beta = \frac{N_{tot} - D_{in}}{N_{tot}}. \quad (1)$$

Here, N_{tot} is the total number of in-region events and D_{in} is the number of in-region events detected by the region-specific detector. We also want to calculate the non-target detection rate γ (detection declared for signal from non-target region)

$$\gamma = \frac{D_{out}}{D_{in} + D_{out}}. \quad (2)$$

Here, D_{out} is the total number of events not from the region but detected by the region-specific detector.

We use the H&S bulletin for these calculations, but we are limited in the strength of our assessments. Hardebeck and Shelly (2016) noted that a few thousand aftershocks were identified, but only about a quarter of them were reliably located. They also note that the formal uncertainty in absolute event location is likely an underestimate. The lack of comprehensiveness means that detections that do not associate to the bulletin cannot be evaluated. Instead, we are limited to calculation of the approximate missed detection rate $\hat{\beta}$ and the approximate non-target detection rate $\hat{\gamma}$:

$$\hat{\beta} = \frac{\widehat{N}_{tot} - \widehat{D}_{in}}{\widehat{N}_{tot}}. \quad (3)$$

$$\hat{\gamma} = \frac{\widehat{D}_{out}}{\widehat{D}_{in} + \widehat{D}_{out}}. \quad (4)$$

$\widehat{N}_{tot}$ is the total number of H&S events in the region after removal of association conflicts (see below), $\widehat{D}_{in}$ is the number of associated in-region events detected by the region-specific detector, $\widehat{D}_{out}$ is the number of out-of-region events associated to the region-specific detector.

The total number of detections produced by a single region-specific detector is given by:

$$\widehat{D}_{tot} = \widehat{D}_{in} + \widehat{D}_{out} + \widehat{D}_{un} . \quad (5)$$

Here $\widehat{D}_{un}$ is the number of unassociated detections by the region-specific detector.

Although $\hat{\beta}$ and $\hat{\gamma}$ are likely poor estimates because of the GT limitations, we are mainly concerned with comparing the performance of the detectors operated individually to their performance as part of the GLRT detector and we expect that the limitations in ground truth affect each approach to the same extent.

Associating detections to clusters

A total of 2519 detections were produced from 6645 triggers by the 12 subspace detectors listed in Table 1 (Configurations 1 and 2). By visual inspection we determined that 19 of the 2519 detections were for non-seismic artifacts. The remaining detections all appear to be for valid seismic signals.

We associated the detection times with the expected arrival times at NHC of the events in the H&S bulletin using the criterion that the expected arrival time be within ± 5 seconds of our detection time. In most cases this tolerance results in a 1-1 mapping. However, there are 11 pairs of events in the H&S bulletin that have expected arrival times within 5 seconds of one another and that belong to different clusters. These are listed in Table S2 of the Electronic Supplement. To avoid association conflicts, we associate the events that occurred closest in time to the detection and remove from consideration the events listed in column 2 labeled “EVID_1”.

Non-target Detections

Table 3 contains the detection results for the 12 detectors when operated independently of one another (Configuration 1). Each row summarizes results by cluster and the last row contains the overall statistics. The overall approximate non-target detection rate ($\hat{\gamma}$) is 59.2%. The detectors contributing the most non-target detections are from the central part of the sequence where inter-

cluster spacing is short. In addition, these detectors have generally lower TBP than those for the northern and southern clusters.

Table 4 contains the detection results for the matched region detector operated as a GLRT detection processor (Configuration 2). Each row summarizes results by cluster and the last row contains the overall statistics. The overall non-target detection rate ($\hat{\gamma}$) is 5.7%. This is an approximate 10-fold reduction relative to operating detectors independently.

The non-target detection rate of 5.7% understates the effectiveness of the GLRT configuration. For purposes of implementing a matched region detector, it is ideal for all detected events to be within one cluster radius. However, association of events at somewhat greater distances could still be of significant utility. Therefore, it is of interest to consider how association varies as a function of separation from cluster centers.

This is illustrated in Figure 5. We computed for each associated detection the distance from the epicenter to the centroid of the cluster for which the detector was built. The blue histogram is the distribution of those distances for detectors operated independently and the red histogram shows the results for GLRT operation. The dashed line is the average of the cluster radii (2.7 km). These are determined by computing the distance of each cluster epicenter from the centroid and taking the maximum of that set.

For the GLRT configuration (Configuration 2), 37 (3.4%) epicenters are more than 1 cluster radius removed from their cluster centroid and only 15 (1.4%) are separated by more than 2 radii. Harris (1991) demonstrates the propensity of low TBP signals to correlate by chance (e.g. signals with TBP = 10 require a ~0.65 correlation threshold to maintain a 1% false detection rate), thus

complicating accurate event attribution at regional to local scales where it is often difficult to increase signal TBP. In addition to contributing to the non-target detection rate, the very low TBP of some detectors contributed to the false detection of the 19 non-seismic artifacts mentioned previously.

We also looked at the effect of removing the noisier and mixed signals from the basis used to construct each of the 12 detectors. Though the number of signals used in building the subspace detectors was lower, the ranks were similar. For some clusters, the total detection count was much lower, but the GLRT performed equivalently in detecting the subspace basis signals. Overall, the careful pruning avoided more non-target detections, but at the expense of a much smaller proportion of the full bulletin. It is most likely that the main cause of non-target detections is that each cluster contains a variety of low TBP signals.

Missed Detection Rate Analysis

For single-detector operation (Configuration 1) the overall missed detection rate ($\hat{\beta}$) is 10.8%. The worst-performing detectors were for the three northern-most clusters. These detectors essentially detected nothing outside their basis signals. Interestingly, for the GLRT operation, the missed detection rate is 13.1%, which is slightly higher than was the case when detectors were operated independently.

To investigate this non-intuitive fact, we look at a case where an individually operated detector detected a target event, but the GLRT failed to make a target detection. Event 82437742 belongs to cluster 5. Four component detectors triggered on this event and are summarized in Table 5. The trigger produced by detector 455639 (the detector corresponding to cluster 5) was not promoted to detection (i.e., not detected by the cluster 5 detector in the GLRT schema) because

its detection statistic was lower than that of the trigger produced by the detector corresponding to cluster 9. In other words, this is a non-target detection. However, our definition of a missed detection lumps together the case where the GLRT fails to detect any signal with the case where the GLRT assigns the detection to the wrong region. In this case both detectors are highly adaptable (high rank), have low TBP, and have large projections on (correlation with) one another. Although the signal from event 82437742 was used in creating detector 455639, apparently enough of its energy ended up in the null space of the singular value decomposition that it was possible for detector 455647 to get a better fit to the signal.

Comparative Performance of Numerous Low-Rank Detectors

We repeated the experiment, this time allowing the DFTT to build its own correlation and subspace detectors where waveform clustering was performed using a correlation threshold of 0.9. for each of the 12 bulletins. This led to the creation of 664 low-rank (maximum rank of 6) detectors across all 12 clusters, with 491 of these detectors being singletons (i.e., correlation detectors). These detectors are summarized in Table 2.

For the single-detector operation (Configuration 3), the overall non-target detection rate ($\hat{\gamma}$) was 32.6% and the overall missed detection rate ($\hat{\beta}$) was 21.0%. For the GLRT operation (Configuration 4) these values were 4.8% and 23.1%, respectively. For both configurations we see that while $\hat{\gamma}$ is lower in this experiment, $\hat{\beta}$ is nearly twice that of the initial experiment (Configurations 1 and 2). Overall, roughly 120 fewer H&S events were correctly detected ($\widehat{D}_{in}$) by each operation in this experiment than in the original. Configuration 3 results are presented in Table 6 and Configuration 4 results are shown in Table 7. A map view plot comparing the results of the two experiments for Cluster 6 is shown in Figure 6. For map view plots comparing the

results of the two experiments for the other clusters, see Figures S1 – S11 in the Electronic Supplement to this article.

Discussion

In this work we introduce the concept of a matched region detector for use in a global monitoring system. Such detectors could potentially improve associator performance because their detections would be accompanied by region information which could be used to constrain hypotheses formed by the associator. We do not envision matched region detectors as a replacement for the incoherent detectors currently used in monitoring systems. Instead, we think such detectors could make event building more robust by taking advantage of more of the information in detected signals. For example, Sundermier et al. (2021) have demonstrated the utility of screening mining signals using correlation detectors. In their work, the correlation detectors do not act as primary detectors, but are rather used to screen detections made by the automatic detectors of the International Monitoring System (IMS). Analogously, a matched region detector would not be a primary source of detections input to the associator. Rather, it would provide hints to the associator that would allow more robust hypothesis generation.

We implement a small-scale test of a matched region detector using aftershocks of the Napa 2014 M_w 6.0 earthquake and Hardebeck and Shelly's (H&S; 2016) double-difference catalog of the aftershocks as quasi ground truth. Our implementation defined 12 regions based on clusters identified by (H&S; 2016). We conducted two experiments (Configurations 1 and 2 vs. Configurations 3 and 4). In each we created a Generalized Likelihood Ratio Test (GLRT) detector from the aftershock signals and then analyzed its performance when applied to the continuous waveform data. In Configurations 1 and 2 we implemented the detector with 12 high-

409 rank subspace detectors each built using the waveforms from a single cluster. In Configurations
410 3 and 4 we implemented the detector using 664 low-rank subspace and correlation detectors,
411 each tied to the cluster from which its basis was chosen.

412 For each experiment we computed the non-target detection rate ($\hat{\gamma}$) and the missed detection rate
413 ($\hat{\beta}$) for the GLRT configurations and for the individual detectors composing the GLRTs. Both
414 experiments show that the GLRT operation gives significantly lower (~10-fold reduction) non-
415 target detection rates than the individually operating detectors, although the missed detection rate
416 is slightly higher for the GLRT configuration. (The higher missed detection rate of the GLRT
417 configuration occurs because non-target detections are counted as missed detections in our
418 analysis.)

419 Non-target detections are more likely to be made when signals have low time bandwidth
420 products, as is certainly the case for most of the detectors in our experiments (Harris, 1991).
421 Harris (1991) demonstrated that increasing the length of available data or the size of the
422 passband greatly reduces the probability of false attribution at fixed correlation thresholds and
423 suggests using data from multiple sensors. We show in Figure 5 that a GLRT detector can also
424 be an effective approach to reducing non-target detections even with low TBP component
425 detectors. In fact, the detectors used here are so marginal that our results are remarkable. Our
426 results are sufficiently encouraging that we think it worthwhile to test the performance of a
427 matched region detector in a configuration more closely resembling that required for a global
428 monitoring system such as the International Monitoring System (IMS).

429 The IMS includes many seismic arrays, and there are several advantages of developing and
430 testing a matched region detector that uses IMS array data and is specialized to regional signals.

An operational implementation at the regional scale would use multi-channel templates many tens of seconds long, which would comparatively have much higher TBP. We have built thousands of subspace detectors using data recorded by IMS arrays and find that templates built using wide passbands and windows that include all regional signals typically have TBP ≥ 150. In some cases (e.g., ARCES array in northern Norway) TBP can exceed 1000. Such detectors are quite resistant to non-target detections. Because of the sensitivity of seismic arrays (relative to 3-component stations) a large fraction of the IDC standard event list (SEL1) detections is by arrays. Therefore, we could expect to have the greatest impact on associator performance by concentrating our efforts on the arrays. Another important benefit of using array data is that we can filter by slowness in choosing signals to incorporate into a detector. This helps minimize the chance of including non-target signals into detector construction. We thus expect such a system to perform much better in terms of false, and non-target, rates when scaled up in this way.

Our expectation of better results at regional distances may initially seem to oppose the observation of Dodge and Walter (2015) that correlation results improved as observation distances decreased. The time bandwidth product of a seismic signal is strongly influenced by both attenuation and scattering. Filtering due to attenuation does lower TBP as observation distances increase, however, at local distances much of the signal complexity is due to scattering. At the very short observation distances we are working with here, waveforms are less complex (less sampling of Earth) and have very short durations (a few seconds). As observation distances increase to a few tens of kilometers, signal complexity and duration increase, increasing signal TBPs.

Our results show that the approach using a few high-rank subspace detectors outperformed the one implementing many low-rank detectors (mostly correlators) in terms of missed detection rate. This agrees with the findings of others (e.g., Kvaerna et al., 2014) and subspace detector theory: Subspace detectors are better able to detect events from within the region sampled by their constituent source events than would be the case for correlation detectors built from the same events.

Configuration 2 (GLRT composed of 12 high-rank subspace detectors) produced a total of 2519 detections, but we could only classify 1090 of them. This limitation was due to the incompleteness of the H&S catalog. Hardebeck and Shelly (2016) note that they detected many more events but were unable to reliably locate them. Thus, for the purpose of quantifying the GLRT performance, we were unable to evaluate detections that did not associate to the bulletin. However, given the low non-target detection rate of the GLRT detector, it is very likely that the unassociated detections are part of the Napa aftershock sequence. Additionally, the H&S location uncertainties are likely underestimates of absolute locations, allowing detectors to be built that included signals from other clusters. We also note that though we did not limit the rank when creating detectors, doing so for sparse clusters will make the resulting detectors less sensitive to outlier signals.

We think this work has shown that there is great promise for the construction and effectiveness of a matched region detector at regional scale. In the next phase of our work, we plan to test the behavior of a matched region detector built with signals from regional events recorded at an IMS array. We will target the aftershock sequence of the 2005 M 7.6 Kashmir earthquake sequence recorded at IMS primary array MKAR. Using the catalog of relocated aftershocks by Gibbons

and Kvaerna (2017), we will test the ability of a GLRT detector to properly regionalize detections. The approach will be like that used in this paper.

In a follow-on study, we will add the non-IMS array KKAR to examine the issue of cross-talk. Will multiple matched region detectors produce consistent results, or will some kind of voting be necessary in order to avoid confusing the associator?

Future work with this system must also address the effectiveness of a GLRT detector built using an incomplete basis. This is a requirement to be useful as part of a permanent monitoring system or for use in aftershock processing where signals collected early in an evolving sequence will be used in processing the latter part of the sequence. So, if the previously mentioned research indicates that matched region detectors are viable using IMS arrays and regional signals, then we will attempt to determine their behavior at various levels of pre-mainshock seismic activity.

Data and Resources

The dynamic correlation processor software has been released as open source under the name Detection Framework Testbed and Toolkit (DFTT) at https://github.com/LLNL/DFTT. The Northern California Seismic Network (NCSN) waveform data for this study were accessed through the Northern California Earthquake Data Center (NCEDC), doi:10.7932/NCEDC (last accessed July 2020). Earthquake locations were provided by Jeanne L. Hardebeck and David R. Shelly. Figure 2 was created using the Generic Mapping Tools (https://www.generic-mapping-tools.org/, last accessed February 2021; Wessel et al., 2013). MATLAB release 2020a was used for analysis and to produce Figures 4 and 6, and S1 – S11 (https://www.mathworks.com/products/matlab.html, last accessed October 2021). Supplemental Content: A table summarizing the Hardebeck and Shelly (2016) event clusters used in this study,

a table summarizing detection-bulletin association reconciliation, and map view figures of the results for all clusters from experiments 1 and 2.

Acknowledgements

We thank Dave Harris for discussion, theoretical development regarding generalized likelihood ratio test detectors, and work on dynamic correlation processors. We thank Jeanne Hardebeck and David Shelly for sharing their earthquake catalog. We also thank Bill Walter and Susan Bilek for helpful comments and support.

This work was performed in part under the auspices of the U.S. Department of Energy by Lawrence Livermore National Laboratory under Contract DE-AC52-07NA27344. Lawrence Livermore National Security, LLC.

References

Carmichael, J. D. (2016). A waveform detector that targets template-decorrelated signals and achieves its predicted performance, Part I: Demonstration with IMS data, Bull. Seismol. Soc. Am., 106, 1998 – 2012.

Carmichael, J. D., and H. Hartse (2016). Threshold magnitudes for a multichannel correlation detector in background seismicity, Bull. Seismol. Soc. Am, Vol. 106, no. 2, pp. 478 – 498, doi:10.1785/0120150191.

Chen, T., S. Lu, P. Qian, G. Chen, and N. Hu (2020). An automatic detection method for 40-Hz auditory steady state response and its application in prognosis of comatose patients, Clinical Neurophysiology, Vol. 131, pp. 703 – 715.

Cleveland, K. M., and C. J. Ammon (2013). Precise relative earthquake location using surface waves, J. Geophys. Res.: Solid Earth, Vol. 118, 1-12, doi:10.1002/jgrb.50146.

Dodge, D. A. and D. B. Harris (2016). Large-Scale Test of Dynamic Correlation Processors: Implications for Correlation-Based Seismic Pipelines, Bull. Seismol. Soc. Am., Vol. 106, No. 2, pp. 435-452.

Dodge, D. A. and W. R. Walter (2015). Initial Global Seismic Cross-Correlation Results: Implications for Empirical Signal Detectors, Bull. Seismol. Soc. Am., Vol. 105, No. 1, pp. 240-256.

Fisk, M. D., H. L. Gray, and G. D. McCartor (1993). Applications of Generalized Likelihood Ratio Tests to Seismic Event Identification, Philips Laboratory, Hanscom Air Force Base, Massachusetts, PL-TR-93-2221.

Fremont, M. J. and S. D. Malone (1987). High precision relative locations of earthquakes at Mount St. Helens, Washington, J. Geophys. Res., 92, 10, 233-10,236.

Geller, R. J. and C. S. Mueller (1980). Four similar earthquakes in central California, Geophys. Res. Lett. 7, 821-824.

Gibbons, S. J. and K. Tormond (2017). Illuminating the seismicity pattern of the October 8, 2005, M = 7.6 Kashmir earthquake aftershocks, Physics of the Earth and Planetary Interiors, Vol. 270, pp. 1-8. doi: 10.1016/j.pepi.2017.06.008.

Gray, H. L., J. Baek, W. A. Woodward, J. Miller, and M. Fisk (1996). A bootstrap generalized likelihood ratio test in discriminant analysis, Computational Statistics & Data Analysis, Vol. 22, pp. 137-158.

Hardebeck, J. L. and D. R. Shelly (2016). Aftershocks of the 2014 South Napa, California, Earthquake: Complex Faulting on Secondary Faults, Bull. Seismol. Soc. Am., Vol. 106, No. 3, pp. 1100-1109.

Harris, D.B. (1991). A Waveform Correlation Method for Identifying Quarry Explosions, Bull. Seismol. Soc. Am., Vol. 81, No. 6, pp. 2395-2418.

Harris, D.B. (2006). “Subspace Detectors: Theory,” Lawrence Livermore National Laboratory Technical Report UCRL-TR-222758, 46 pages, Livermore, CA.

Harris, D. B. and D. A. Dodge (2011). An Autonomous System for Grouping Events in a Developing Aftershock Sequence, Bull. Seismol. Soc. Am., Vol. 101, No. 2, pp. 763-774.

Harris, D. B. and T. Paik (2006). Subspace Detectors: Efficient Implementation, Lawrence Livermore Natl. Lab. Rep. UCRL-TR-223177, 36 pp.

Harris, D. B. (2019). personal communication. (Theoretical development notes)

Harris, D. B. and D. A. Dodge (2021). The geometry of signal space: a case study of direct mapping between seismic signals and event distribution, *Geophys. J. Int.*, Vol. 224, No. 3, pp. 2189–2208, https://doi.org/10.1093/gji/ggaa572.

Hauksson, E. and P. Shearer (2005), Southern California hypocenter relocation with waveform cross-correlation, Part 1: Results using the double difference method, Bull. Seismol. Soc. Am., 95, 896-903.

Kim, H., M. P. Nguyen, and S. Y. Chun (2017). Cancelable ECG Biometrics using GLRT and Performance Improvement using Guided Filter with Irreversible Guide Signal, 39th Annual Int. Conf. IEEE Engineering in Medicine and Biology.

Kim, J-S., H. Nam, H. J. Kim, J. H. Lee, and B. H. Park (2019). Real-Time Measurement of Ammonia (NH3) in Artillery Smoke Using a Passive FT-IR Remote Sensor, ACS Omega, Vol. 4, pp. 16768-16773.

Kværna, T., D. B. Harris, S. J. Gibbons, D. A. Dodge (2014). Adapting Pipeline Architectures to Track Developing Aftershock Sequences and Recurrent Explosions, AFRL-RV-PS-TR-2014-0075, AFRL Space Vehicles Directorate.

564 Nan, F. Y. and R. D. Nowak (1999). Generalized Likelihood Ratio Detection for fMRI Using
565 Complex Data, IEEE Trans. Medical Imaging, Vol. 18, No. 4, pp. 320 – 329.
566 NCEDC (2014). Northern California Earthquake Data Center. UC Berkeley Seismological
567 Laboratory. Dataset. Doi:10.7932/NCEDC.

568 Neyman, J. and E. S. Pearson (1928). On the Interpretation of Certain Test Criteria for Purposes
569 of Statistical Inference: Part II, Biometrika, Vol. 20A, No. 3/4, pp. 263-294.

570 Ringdal, F., S. J. Gibbons, and D. B. Harris (2008). ADAPTIVE WAVEFORM
571 CORRELATION DETECTORS FOR ARRAYS: ALGORITHMS FOR AUTONOMOUS
572 CALIBRATION in 2008 Monitoring Research Review: Ground-Based Nuclear Explosion
573 Monitoring Technologies.

574 Schaff, D. P. (2009). Broad-scale applicability of correlation detectors to China seismicity,
575 Geophys. Res. Lett., 36, L11301, doi:10.1029/2009GL038179.
576 Schaff, D. P. and P. G. Richards (2004). Lg-wave cross correlation and double-difference
577 location: application to the 1999 Xiuyan, China, sequence, Bull. Seism. Soc. Am., Vol. 94., pp
578 867–879.

579 Schaff, D. P. and P. G. Richards (2004). Repeating seismic events in China, Science, 303, pp.
580 1176-1178.

581 Slinkard, M., D. Schaff, N. Mikhailova, S. Heck, C. Young, and P. G. Richards (2014).
582 Multistation validation of waveform correlation techniques as applied to broad regional
583 monitoring, Bull. Seismol. Soc. Am., Vol. 104, No. 6, pp. 2768-2781. doi: 10.1785/0120140140.

Slinkard, M., S. Heck, D. Schaff, N. Bonal, D. Daily, C. Young, P. G. Richards (2016). Detection of the Wenchuan Aftershock Sequence Using Waveform Correlation with a Composite Regional Network, *Bull. Seismol. Soc. Am.,* Vol. 106, No. 4, pp. 1371–1379. doi: https://doi.org/10.1785/0120150333.

Sundermier, A., R. Tibi, R. A. Brogan, and C. J. Young (2021). Applying Waveform Correlation to Reduce Seismic Analyst Workload Due to Repeating Mining Blasts, Bull. Seismol. Soc. Am., doi: 10.1785/0120210124.

Taylor, S. R. and H. E. Hartse (1997). An Evaluation of Generalized Likelihood Ratio Outlier Detection to Identification of Seismic Events in Western China, Bull. Seismol. Soc. Am., Vol. 87, No. 4, pp. 824-831.

Van Trees, H. L. (1968). *Detection, Estimation and Modulation Theory*, Vol. 1, John Wiley and Sons, New York, New York.

Wang, Z. (2020). Adaptive Detection of a Subspace Signal in Structured Random Interference Plus Thermal Noise, Circuits, Systems, and Signal Processing.

Wang, P. and H. Li (2020). Target Detection with Imperfect Waveform Separation in Distributed MIMO Radar, IEEE Trans. Signal Processing, Vol. 68, pp. 793 – 807.

Wessel, P., W. H. F. Smith, R. Scharroo, J. Luis, and F. Wobbe (2013). Generic Mapping Tools: Improved version released, *Eos Tras. AGU* 94, no. 45, 409-410, doi: 10.1002/2013EO450001.

Mailing Addresses

Rhiannon E. Vieceli

Corresponding Author

Earth and Environmental Science Department

New Mexico Institute of Mining and Technology

801 Leroy Place

Socorro, New Mexico 87801

rhiannon.vieceli@student.nmt.edu

(R.E.V.)

Douglas A. Dodge

Lawrence Livermore National Laboratory

7000 East Avenue

Mail Stop 046

Livermore, California 94550

dodge1@llnl.gov

(D.A.D)

Tables

Table 1 Detector Summary Results for Configurations 1 and 2. For each cluster we extracted waveform segments for each cluster event. The totals are listed in column 2. Column 3 contains the totals of signals remaining after removal of segments with quality problems. The fourth column (Detector Rank) contains the number of singular values retained for each of detectors.

Cluster	Cluster Event Count	Signals used	Detector Rank	Distance (km) from NHC	Detector Time Bandwidth Product
1	47	33	25	15.93	19.81
2	79	65	42	12.75	4.85
3	101	68	47	10.37	6.74
4	170	138	61	6.87	3.12
5	91	80	41	3.79	2.47
6	176	112	36	2.68	0.68
7	155	115	37	3.06	1.26
8	47	34	22	1.88	4.7
9	158	115	34	3.38	1.12
10	77	59	26	3.84	4.36
11	30	26	15	4.88	3.31
12	63	46	29	7.35	5.49
All	1194	891			

Table 2 Detector Summary Results for Configurations 3 and 4. For each cluster we extracted waveform segments for each cluster event. The totals are listed in column 2. Column 3 contains the totals of signals used in DFTT correlation and subspace detector creation. These numbers may be larger than the catalog numbers because DFTT was allowed to create its own detectors using catalog event times; additional events not in the particular cluster catalog may have been pulled in. The fourth column (Detectors) contains the number of detectors created for each cluster. Column 5 contains the maximum rank among the detectors of column 4.

Cluster	Cluster Event Count	Signals used	Detectors	Maximum Detector Rank
1	47	30	25	3
2	79	47	38	3
3	101	58	51	2
4	170	120	107	2
5	91	96	66	5
6	176	200	86	6
7	155	179	93	6
8	47	40	31	3
9	158	152	78	5
10	77	86	37	6
11	30	34	14	3
12	63	51	38	2
All	1194	1093	664	

Table 3 Detection summary for individual detectors when each high-rank detector is operated independently (Configuration 1). The $\widehat{N}_{tot}$ column is the number of Hardebeck and Shelly (H&S; 2016) events in the region after resolving conflicts. The $\widehat{D}_{tot}$ (Total Detections) column lists the total number of detections by each detector independent of any association. The $\widehat{D}_{in}$column is the number of associated H&S events in the region. The $\widehat{D}_{out}$ column is the number of associated H&S events outside the region. $\hat{\beta}$is the missed detection rate as a percentage and $\hat{\gamma}$ is the non-target detection rate.

Cluster	$\widehat{N}_{tot}$	$\widehat{D}_{tot}$	$\widehat{D}_{in}$	$\widehat{D}_{out}$	$\hat{\beta}$	$\hat{\gamma}$
1	47	33	33	0	29.8%	0%
2	79	66	65	1	17.7%	1.5%
3	100	70	67	2	33%	2.9%
4	167	862	155	202	7.2%	56.6%
5	89	1173	86	314	3.4%	78.5%
6	175	1498	160	309	8.6%	65.9%
7	155	1294	148	295	4.5%	66.6%
8	45	335	38	149	15.6%	79.7%
9	157	1040	154	233	1.9%	60.2%
10	76	157	71	15	6.6%	17.4%
11	30	40	27	2	10%	6.9%
12	63	77	51	9	19%	15.0%
	1183	6645	1055	1531	10.8%	59.2%

Table 4 Detection summary for individual detectors when a high-rank matched region detector is operated as a GLRT detector (Configuration 2). The $\widehat{N}_{tot}$ column is the number of Hardebeck and Shelly (H&S; 2016) events in the region after deconflicting. The $\widehat{D}_{tot}$ (Total Detections) column lists the total number of detections by each detector independent of any association. The $\widehat{D}_{in}$column is the number of associated H&S events in the region. The $\widehat{D}_{out}$ column is the number of associated H&S events outside the region. $\hat{\beta}$is the missed detection rate as a percentage and $\hat{\gamma}$ is the non-target detection rate.

Cluster	$\widehat{N}_{tot}$	$\widehat{D}_{tot}$	$\widehat{D}_{in}$	$\widehat{D}_{out}$	$\hat{\beta}$	$\hat{\gamma}$
1	47	33	33	0	29.8%	0
2	79	65	65	0	17.7%	0
3	100	68	67	1	33%	1.5%
4	167	309	154	4	7.8%	2.5%
5	89	233	83	4	6.7%	4.6%
6	175	789	160	15	8.6%	8.6%
7	155	470	137	13	11.6%	8.7%
8	45	39	34	2	24.4%	5.6%
9	157	297	146	20	7.0%	12.0%
10	76	125	71	3	6.6%	4.1%
11	30	36	27	0	10.0%	0
12	63	55	51	0	19.0%	0
	1183	2519	1028	62	13.1%	5.7%

Table 5 Summary of detector triggers for event 82437742. The event belongs to cluster 5 but the detector with the highest detection statistic belongs to cluster 9. Both detectors have a large number of dimensions (41 for 455639 and 34 for 455647) and low time bandwidth product (TBP) per dimension (2.5 for 455639 and 1.1 for 455647) Their projection on (correlation with) one another is very high (0.958). Therefore, their target signal spaces largely overlap.

Detector ID	Detector Cluster	Trigger ID	Detection Statistic	Trigger Promoted to Detection (y/n)
455647	9	27207606	0.738	y
455643	7	27207668	0.725	n
455641	6	27207649	0.675	n
455639	5	27207622	0.604	n

Table 6 Detection summary for individual detectors when each low-rank detector is operated independently (Configuration 3). The $\widehat{N}_{tot}$ column is the number of Hardebeck and Shelly (H&S; 2016) events in the region after resolving conflicts. The $\widehat{D}_{tot}$ (Total Detections) column lists the total number of detections by each cluster's detectors independent of any association. The $\widehat{D}_{in}$column is the number of associated H&S events in the region. The $\widehat{D}_{out}$ column is the number of associated H&S events outside the region. $\hat{\beta}$is the missed detection rate as a percentage and $\hat{\gamma}$ is the non-target detection rate.

Cluster	$\widehat{N}_{tot}$	$\widehat{D}_{tot}$	$\widehat{D}_{in}$	$\widehat{D}_{out}$	$\hat{\beta}$	$\hat{\gamma}$
1	47	36	27	0	42.6%	0%
2	79	84	47	0	40.5%	0%
3	100	69	57	0	43.0%	0%
4	167	177	129	1	22.8%	0.8%
5	89	457	73	85	18.0%	53.8%
6	175	2223	151	55	13.7%	26.7%
7	155	1584	135	125	12.9%	48.1%
8	45	471	33	80	26.7%	70.8%
9	157	952	138	68	12.1%	33.0%
10	76	401	68	34	10.5%	33.3%
11	30	94	27	2	10.0%	6.9%
12	63	77	50	2	20.6%	3.8%
	1183	6625	935	452	21.0%	32.6%

Table 7 Detection summary for individual detectors when a low-rank matched region detector is operated as a GLRT detector (Configuration 4). The $\widehat{N}_{tot}$ column is the number of Hardebeck and Shelly (H&S; 2016) events in the region after deconflicting. The $\widehat{D}_{tot}$ (Total Detections) column lists the total number of detections by each cluster's detectors independent of any association. The $\widehat{D}_{in}$column is the number of associated H&S events in the region. The $\widehat{D}_{out}$ column is the number of associated H&S events outside the region. $\hat{\beta}$is the missed detection rate as a percentage and $\hat{\gamma}$ is the non-target detection rate.

Cluster	$\widehat{N}_{tot}$	$\widehat{D}_{tot}$	$\widehat{D}_{in}$	$\widehat{D}_{out}$	$\hat{\beta}$	$\hat{\gamma}$
1	47	31	27	0	42.6%	0%
2	79	52	47	0	40.5%	0%
3	100	61	57	0	43.0%	0%
4	167	149	128	1	23.4%	0.8%
5	89	190	72	8	19.1%	10.0%
6	175	346	143	6	18.3%	4.0%
7	155	251	128	9	17.4%	6.6%
8	45	55	31	3	31.1%	8.8%
9	157	241	136	13	13.4%	8.7%
10	76	121	64	6	15.8%	8.6%
11	30	53	27	0	10.0%	0%
12	63	58	50	0	20.6%	0%
	1183	1608	910	46	23.1%	4.8%

List of Figure Captions

Figure 1: Notational Matched Region Detector. The domain of the detector is the set of regions enclosed by red squares. Each region has one associated subspace detector built from signals recorded at the station (yellow triangle) from previous events within the region.

Figure 2: Map view of the Napa Valley aftershocks used in this study (locations from Hardebeck and Shelly, 2016). We grouped the events into 12 clusters using a K-means algorithm following visual interpretation of the clusters identified by Hardebeck and Shelly (2016); they are distinguished by different colored circles, black polygons, and cluster number. We analyzed waveforms for these events as recorded at station NHC (black triangle) of the Northern California (NC) network.

Figure 3: Schematic example of creating a single GLRT detector based on six subspace detectors. Each of the constituent subspace detectors is optimized for a specific cluster and although they can produce triggers for adjacent cluster events, they are unlikely to produce detections for non-basis clusters. SVD refers to singular value decomposition. The red dots represent known or cataloged events that comprise the subspace detectors, and the black dots represent additional events that are to be detected.

Figure 4: Basis vectors of the Cluster 6 subspace detector used in Configurations 1 and 2.

Figure 5: shows detection count histograms as a function of distance from associated cluster centroid for non-Generalized Likelihood Ratio Test (non-GLRT) detections (blue) and GLRT detections (red).

675 Figure 6: Map view results of Experiment 1 (Configurations 1 and 2, a few high-rank detectors;
676 left) and Experiment 2 (Configurations 3 and 4, many low-rank detectors; right) for Cluster 6.

Figures

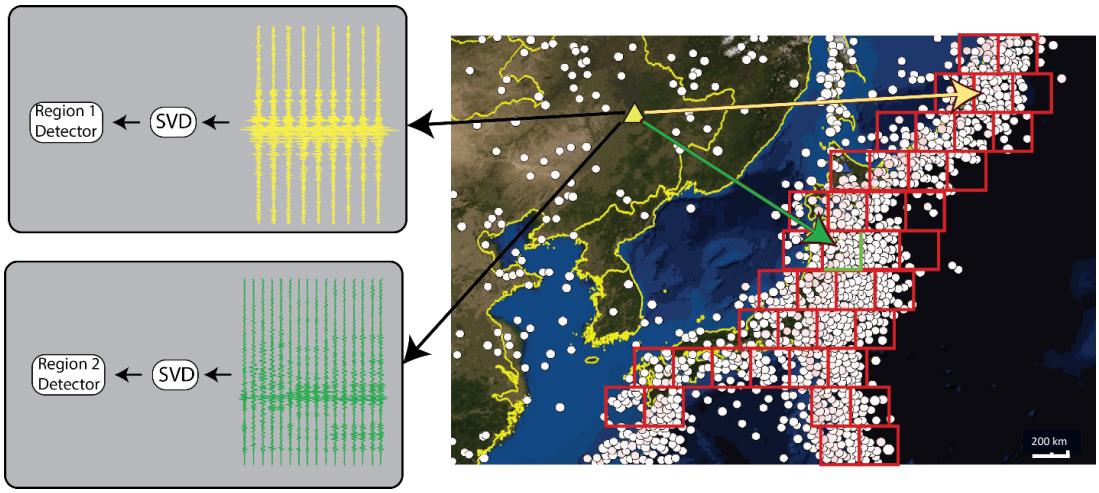

Figure 1 Notional Matched Region Detector. The domain of the detector is the set of regions enclosed by red squares. Each region has one associated subspace detector built from signals recorded at the station (yellow triangle) from previous events within the region.

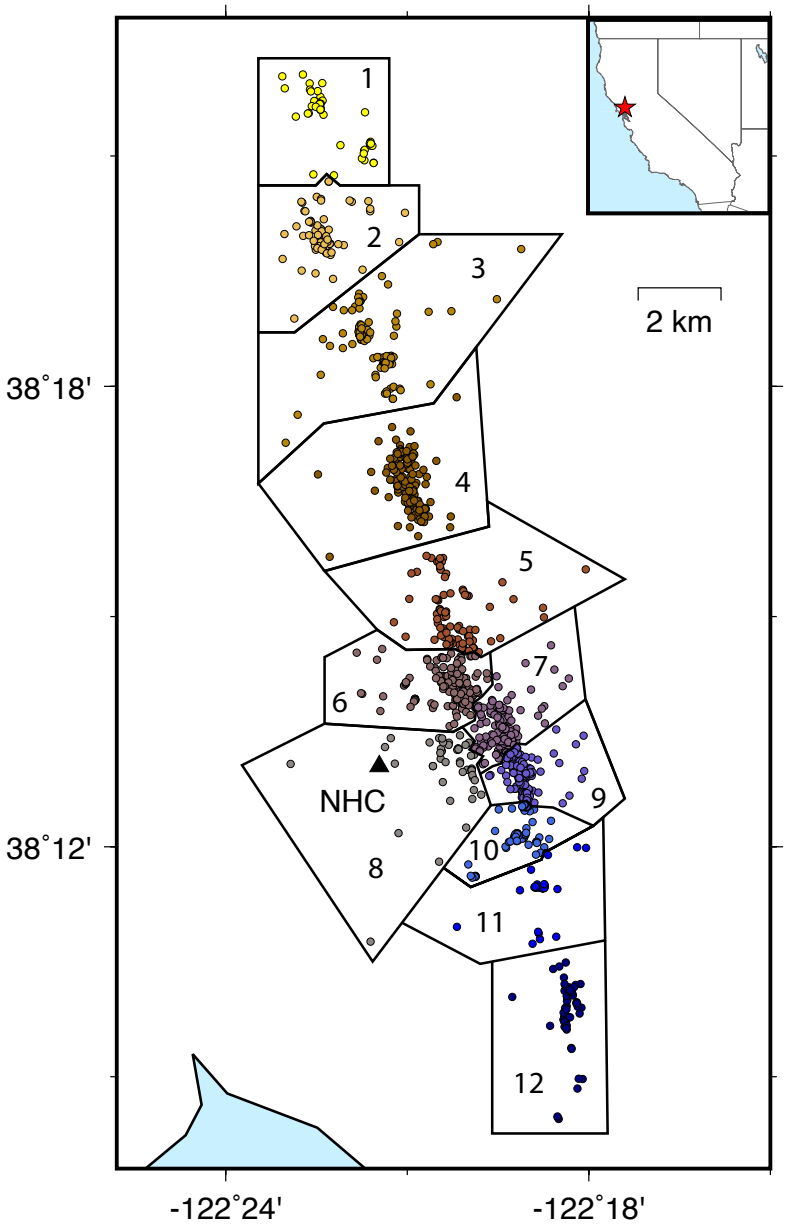

Figure 2 Map view of the Napa Valley aftershocks used in this study (locations from Hardebeck and Shelly, 2016). We grouped the events into 12 clusters using a K-means algorithm following visual interpretation of the clusters identified by Hardebeck and Shelly (2016); they are distinguished by different colored circles, black polygons, and cluster number. We analyzed waveforms for these events as recorded at station NHC (black triangle) of the Northern California (NC) network.

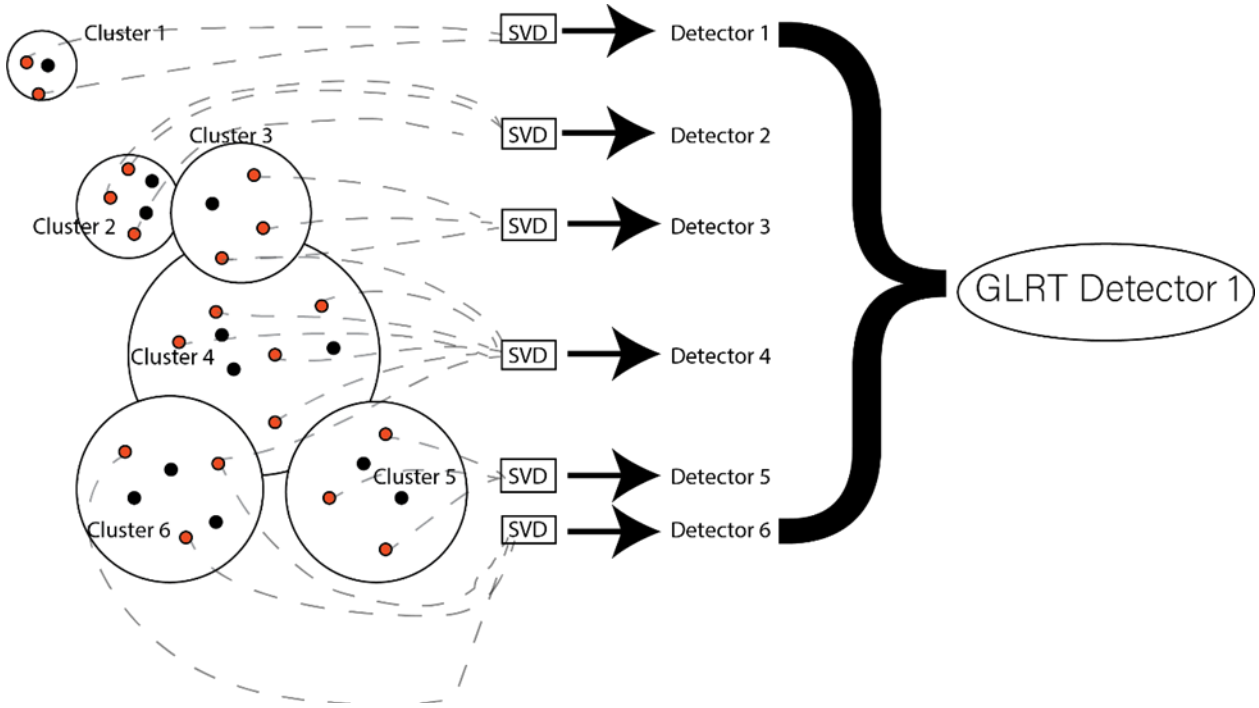

687

688 *Figure 3 Schematic example of creating a single GLRT detector based on six subspace detectors. Each of the constituent*
689 *subspace detectors is optimized for a specific cluster and although they can produce triggers for adjacent cluster events, they are*
690 *unlikely to produce detections for non-basis clusters. SVD refers to singular value decomposition. The red dots represent known*
691 *or cataloged events that comprise the subspace detectors, and the black dots represent additional events that are to be detected.*

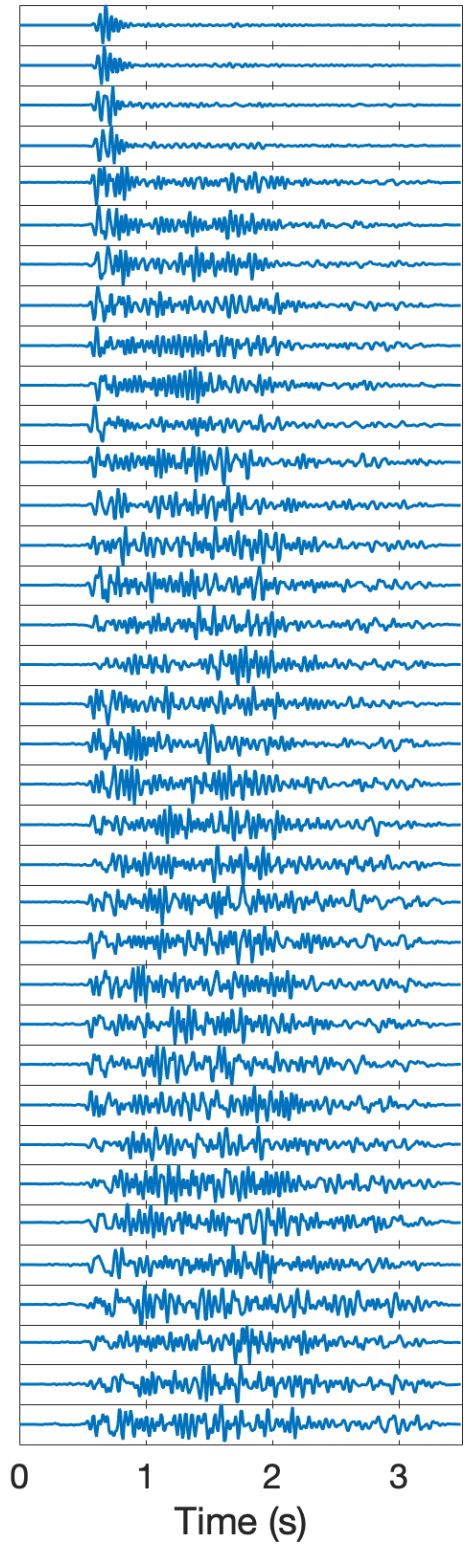

Figure 4 Basis vectors of the Cluster 6 subspace detector used in Configurations 1 and 2.

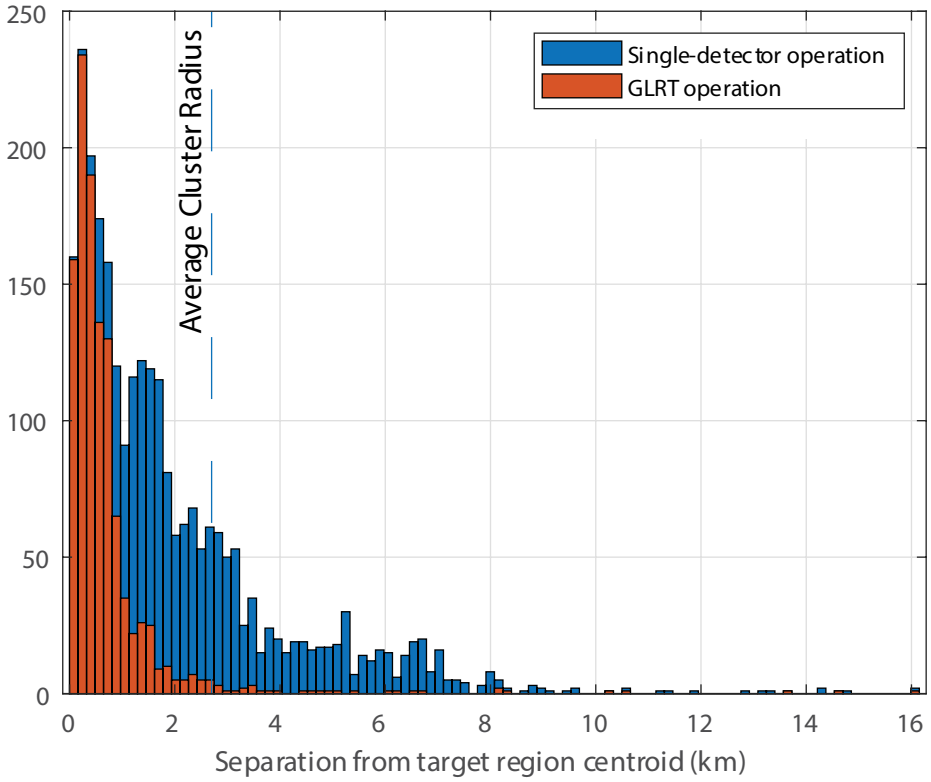

Figure 5 shows detection count histograms as a function of distance from associated cluster centroid for non-Generalized Likelihood Ratio Test (non-GLRT) detections (blue) and GLRT detections (red).

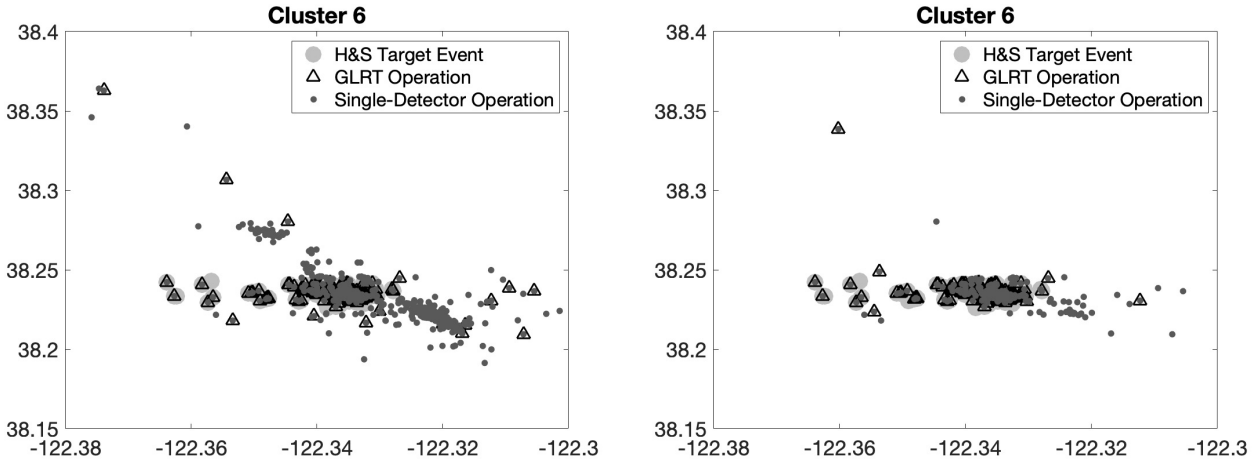

Figure 6 Map view results of Experiment 1 (Configurations 1 and 2, a few high-rank detectors; left) and Experiment 2 (Configurations 3 and 4, many low-rank detectors; right) for Cluster 6.

Electronic Supplement

Table S1 Summary of Cluster data derived from Hardebeck and Shelly (H&S; 2016) bulletin.

Cluster Number (North to South)	Number of Events in Cluster	Centroid latitude	Centroid longitude	Max radius (km)
1	48	38.36016	-122.37386	1.82
2	80	38.33147	-122.37316	2.09
3	101	38.31071	-122.36018	4.2
4	170	38.27892	-122.34944	2.61
5	91	38.24802	-122.33840	3.55
6	178	38.23475	-122.33624	2.55
7	155	38.22442	-122.32375	2.45
8	47	38.21837	-122.33619	4.82
9	160	38.21626	-122.31902	1.77
10	80	38.20225	-122.31824	1.57
11	30	38.19119	-122.31300	2.25
12	63	38.16524	-122.30604	2.72

Table S2 11 event pairs in the Hardebeck and Shelly (H&S; 2016) bulletin with time separations less than 5 seconds and with each event belonging to a different cluster. Shaded events not used in association.

CLUSTERID_1	EVID_1	CLUSTERID_2	EVID_2	SEPARATION (km)	DELTA_T (s)
3	82438514	7	82438517	10.28	1.71982
4	82438462	8	82438464	7.84	1.87712
4	82437977	5	82437980	4.11	2.86089
4	82439563	7	82439568	6.36	3.82249
5	82440305	3	82440309	8.91	4.46571
5	82443447	9	82443450	3.85	3.76529
6	72283306	5	82451735	1.16	-3.82132
8	82468126	4	82468130	9.09	4.55256
8	82442406	2	82442409	13.2	3.6687
9	71086754	5	82439163	4.18	4.11731
10	72282966	8	82439426	2.74	4.26796

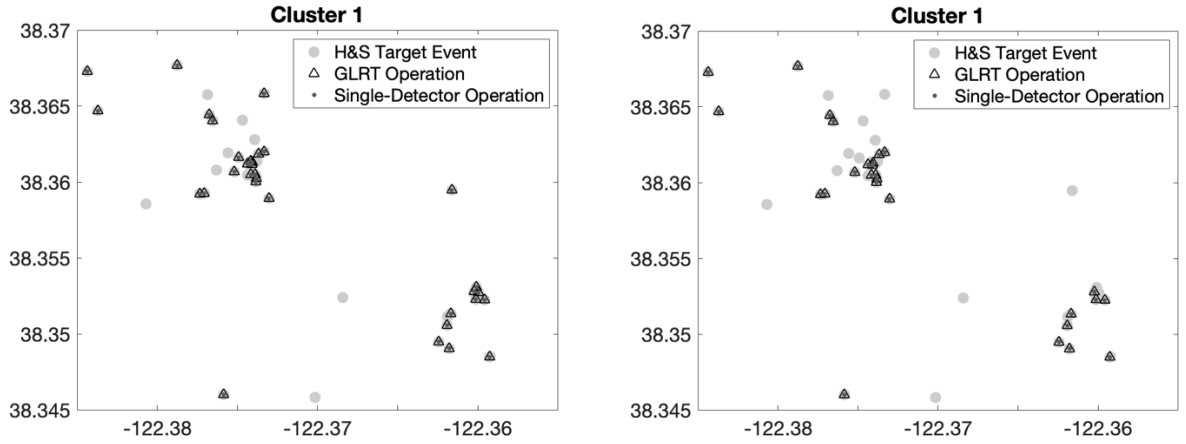

Figure S1 Map view results of Experiment 1 (Configurations 1 and 2, a few high-rank detectors; left) and Experiment 2 (Configurations 3 and 4, many low-rank detectors; right) for Cluster 1.

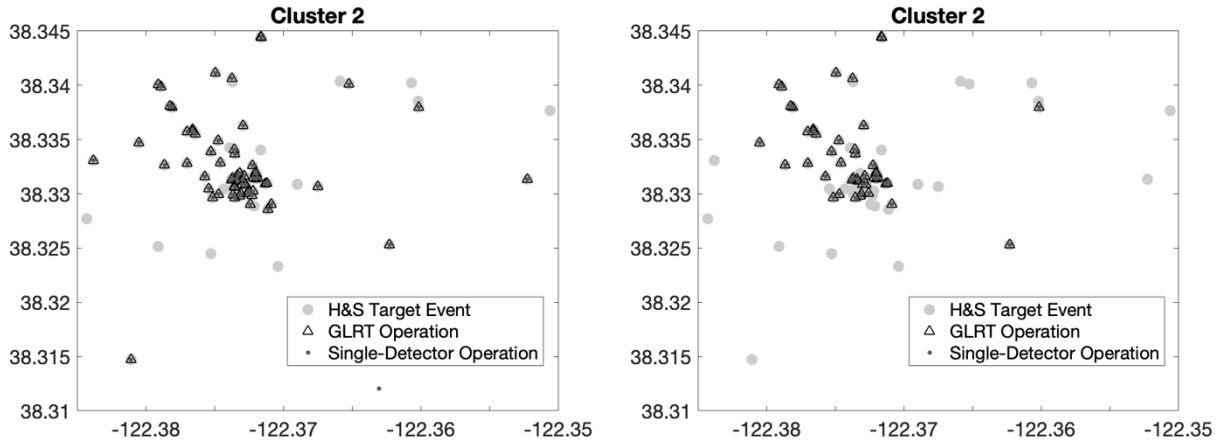

Figure S2 Map view results of Experiment 1 (Configurations 1 and 2, a few high-rank detectors; left) and Experiment 2 (Configurations 3 and 4, many low-rank detectors; right) for Cluster 2.

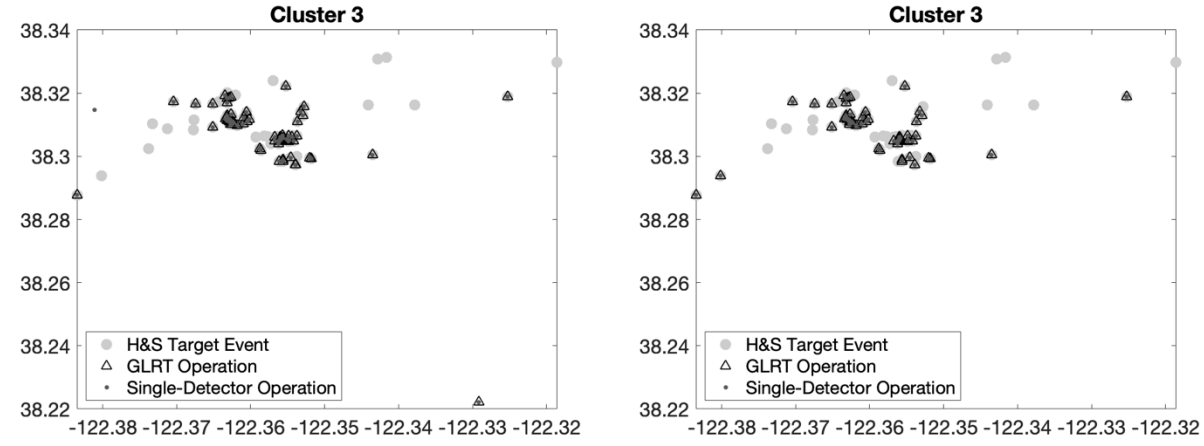

Figure S3 Map view results of Experiment 1 (Configurations 1 and 2, a few high-rank detectors; left) and Experiment 2 (Configurations 3 and 4, many low-rank detectors; right) for Cluster 3.

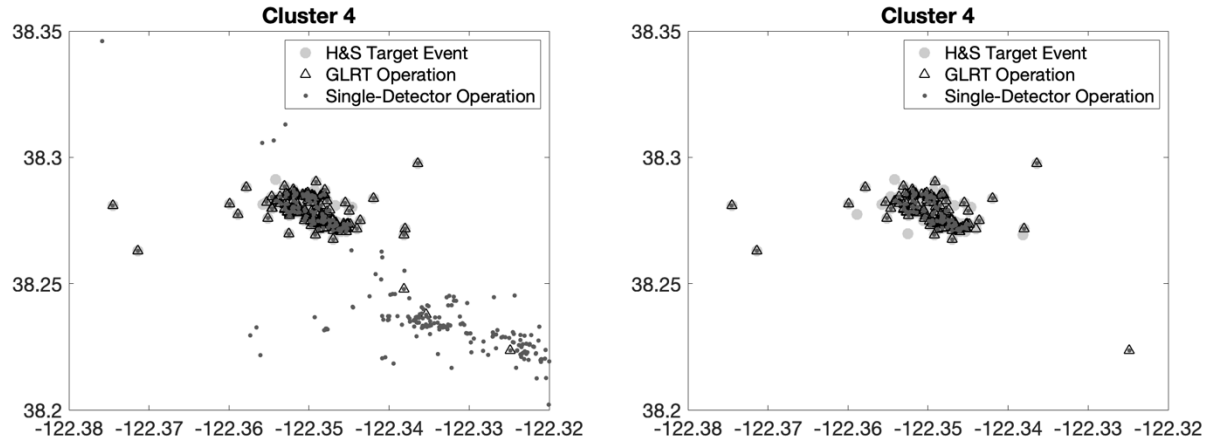

Figure S4 Map view results of Experiment 1 (Configurations 1 and 2, a few high-rank detectors; left) and Experiment 2 (Configurations 3 and 4, many low-rank detectors; right) for Cluster 4.

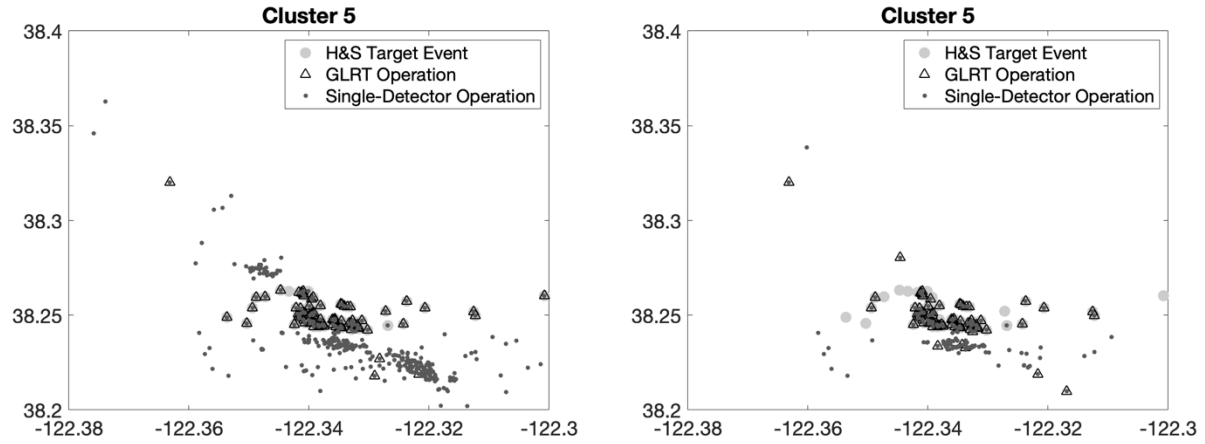

Figure S5 Map view results of Experiment 1 (Configurations 1 and 2, a few high-rank detectors; left) and Experiment 2 (Configurations 3 and 4, many low-rank detectors; right) for Cluster 5.

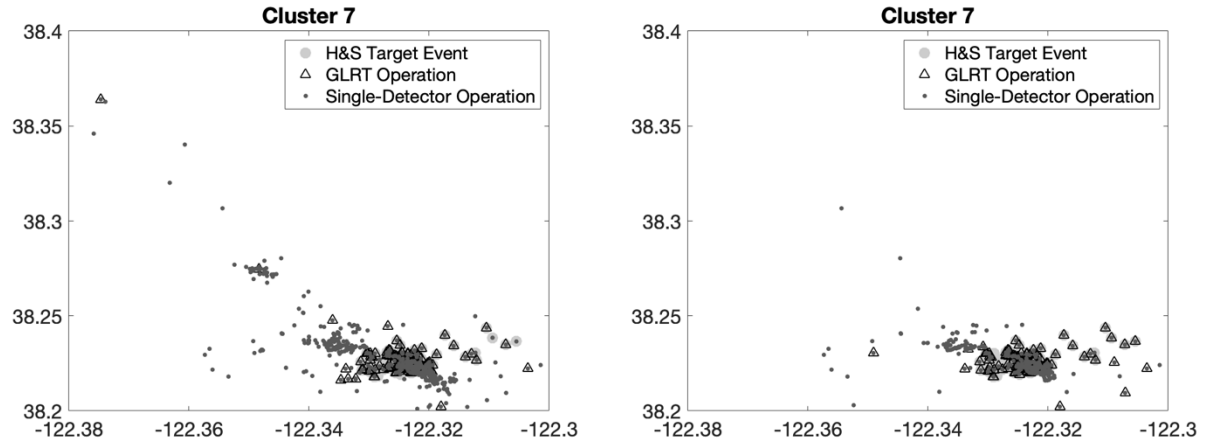

Figure S6 Map view results of Experiment 1 (Configurations 1 and 2, a few high-rank detectors; left) and Experiment 2 (Configurations 3 and 4, many low-rank detectors; right) for Cluster 7.

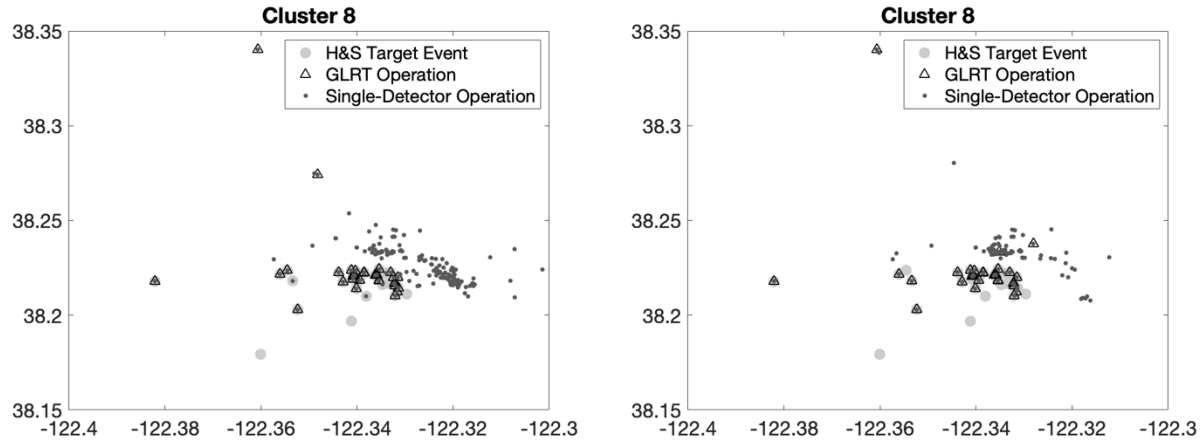

Figure S7 Map view results of Experiment 1 (Configurations 1 and 2, a few high-rank detectors; left) and Experiment 2 (Configurations 3 and 4, many low-rank detectors; right) for Cluster 8.

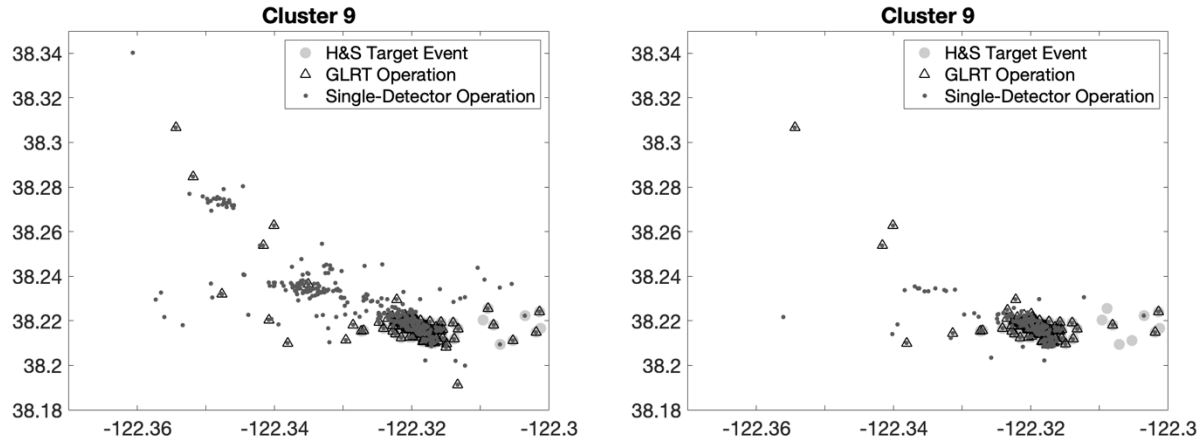

Figure S8 Map view results of Experiment 1 (Configurations 1 and 2, a few high-rank detectors; left) and Experiment 2 (Configurations 3 and 4, many low-rank detectors; right) for Cluster 9.

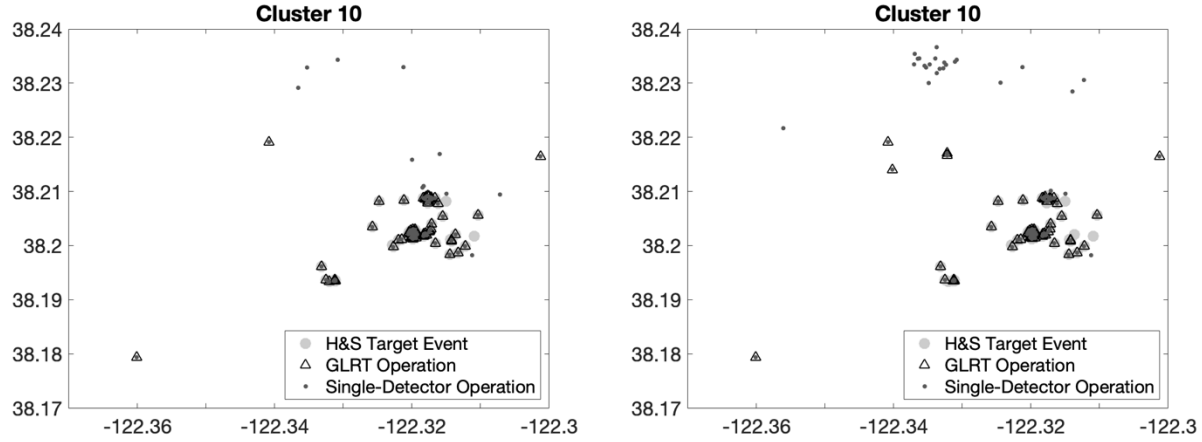

Figure S9 Map view results of Experiment 1 (Configurations 1 and 2, a few high-rank detectors; left) and Experiment 2 (Configurations 3 and 4, many low-rank detectors; right) for Cluster 10.

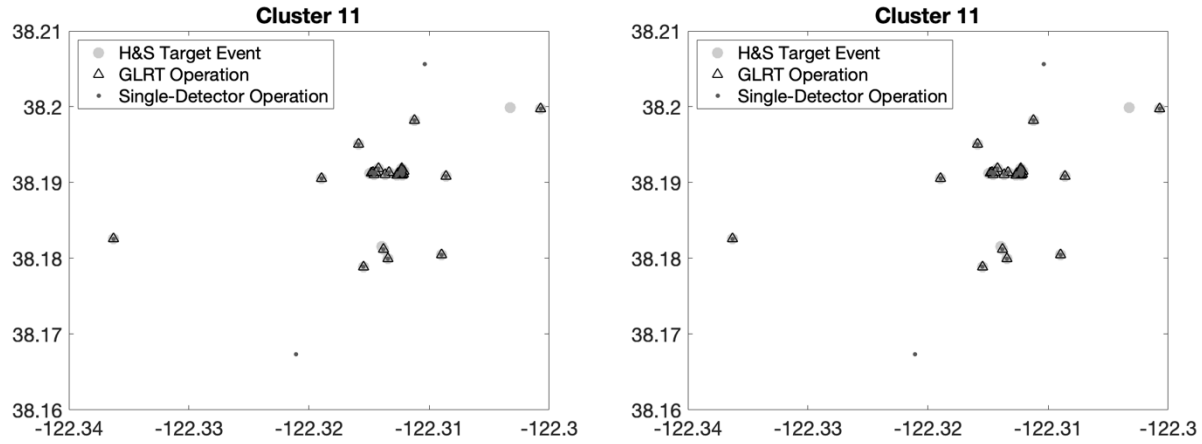

Figure S10 Map view results of Experiment 1 (Configurations 1 and 2, a few high-rank detectors; left) and Experiment 2 (Configurations 3 and 4, many low-rank detectors; right) for Cluster 11.

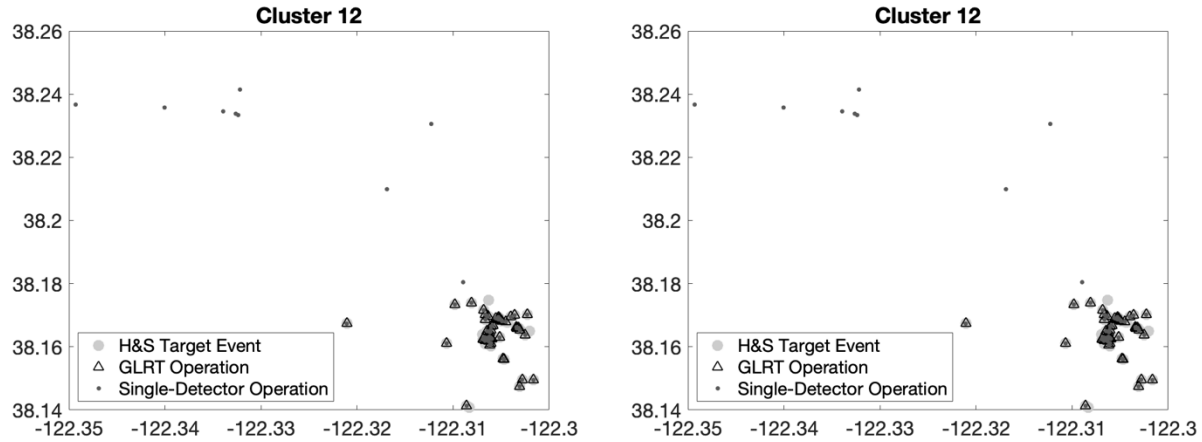

Figure S11 Map view results of Experiment 1 (Configurations 1 and 2, a few high-rank detectors; left) and Experiment 2 (Configurations 3 and 4, many low-rank detectors; right) for Cluster 12.